Asymptotic numerical method for problems coupling several nonlinearities

Hanane Abichou, Hamid Zahrouni, Michel Potier-Ferry

Asymptotic numerical method for problems coupling several nonlinearities

H. Abichou [a,*], H. Zahrouni [b], M. Potier-Ferry [b]

[a] *Ecole Nationale d'Ingénieurs de Tarbes, 47, Av d'Azereix BP 1629-65016 Tarbes Cedex, France*
[b] *LPMM, UMR CNRS 7554, ISGMP, Université de Metz, Ile du Saulcy, 57045 Metz Cedex 01, France*

The objective of this paper is to assess the efficiency of the asymptotic numerical method to solve problems coupling various nonlinearities. The 3D hemispherical stretching of a circular sheet, that involves geometrical, material and red unilateral contact nonlinearities is chosen as an example. An elastoplastic model based on the plasticity deformation theory is adopted. The structural discretization is performed by a shell finite element well adapted for problems involving large displacements and large rotations. The unilateral contact problem is identified to boundary conditions which are replaced by force–displacement relations and solved using a special algorithm. Comparisons with results obtained by the help of an industrial code establish the interest and the performance of the present method.

1. Introduction

We propose an asymptotic numerical method (ANM) to solve problems coupling various nonlinearities. We choose as an example, the numerical simulation of the 3D hemispherical stretching of a circular sheet. This kind of problems involves various nonlinearities due to geometry, plasticity and contact; this leads to a large computing time in the numerical simulation.

The present work is mainly devoted to study the influence of the unilateral contact nonlinearity. This choice is justified by the great complexity of the unilateral contact conditions involved in the numerical simulation. Furthermore, general methods dealing with this kind of problem are usually time consuming [13]. The contact problem is generally solved by minimizing the potential energy and taking into account the equations giving the displacement constraints. Technical difficulties come from the contact regions which are not known prior to the analysis and must be defined from the numerical procedure.

* Corresponding author.
E-mail address: potier-ferry@lpmm.univ-metz.fr (H. Abichou).

To solve such nonlinear problems, one usually uses a predictor–corrector method. This latter consists in following the solution branch in a stepwise manner via a succession of linearizations and of some iterations to achieve the equilibrium. To take into account the contact conditions, generally, two well known formulations are used: the Lagrange multipliers method [8,18] and the penalty method [8,15].

In the Lagrange multipliers method, an additional vector is introduced representing the contribution of the contact forces. So, the contact problem with displacement constraints is replaced by an unconstrained problem but with the vector of Lagrange multipliers as an additional variable. This leads to an augmented stiffness matrix with a dimension which is greater than the one of the initial problem. Numerical difficulties arise since zero terms appear in the diagonal of the stiffness matrix [14] and the computing time increases because of the resulting size of the matrix. The penalty function method introduces an arbitrary penalty number in the energy function to take into account the displacement constraints relation. This number is sufficiently great by comparison with the terms of the stiffness matrix. This method does not increase the size of the stiffness matrix but generates an ill-conditioning of this latter. In the contact literature, there are other methods which are generally based on these two latter techniques.

In this paper, we adopt another way to take into account the contact forces. This is already presented by Elhage et al. [11] in the ANM context for 2D elastic problems. The contact sheet-tools is assimilated to an interaction between a deformable body and a rigid one. This contact problem is identified to boundary conditions which are replaced by force–displacement relationships. In this way, the size of the stiffness matrix does not increase and there is no spurious penetration phenomenon.

The ANM allows us to search solution branches in the shape of power series [6] which can be improved by using a new approximation expressed in terms of rational fractions named Padé approximants [12,17]. Thus, it transforms the nonlinear problem into a recursive sequence of well posed linear problems having the same tangent operator; these latter are generally solved numerically by the finite element method. The ANM is very efficient and easy to implement when the equations of the problem are formulated in a quadratic framework. Then we obtain a part of the solution branch by carrying out only one stiffness matrix decomposition (MD).

The asymptotic expansions have a radius of convergence which limits the validity range of the solution. Consequently, to compute the entire solution branch, it is necessary to apply the ANM in a step by step manner [5].

This method has shown its efficiency to solve problems involving geometrical nonlinearities [5], flow of the viscous fluids [4,25], shell structures with large displacements and large rotations [27], plasticity [1,28], frictionless contact problems [11] and large viscoplastic strains [24].

The constitutive law as well as the contact relations are not analytic and this property is required to apply an asymptotic procedure. To overcome this difficulty, these relations are regularized in such a way that solution curves can be expanded into power series [20].

The aim of this paper is to assess the ability of the ANM to solve problems combining various nonlinearities, as it has been performed in the case of viscoplastic materials [24]. This work will constitute a first step towards a new approach for the numerical simulation of the sheet forming process where the geometrical nonlinearity is coupled with the material one as well as the nonlinearity induced by the contact conditions. It is well known that the contact analysis is numerically the most difficult problem in the metal forming simulation context despite the simplest constitutive relations used. The present contact algorithm contributes to reduce this difficulty by means of a simple technique: there is no modification of the size of the stiffness matrix, the kinematic compatibility condition is respected (no penetration) and the obtained solution path is continuous.

In this study, the unloading is not taken into account. Furthermore we limit ourselves to a frictionless contact problem as well as to simple tool shapes. We are sure that it is possible to introduce friction [2] and various tool shapes [11]. However, an efficient algorithm is not yet available in the case of a consistent plastic material.

2. Basic formulation

The present study is based on the shell formulation proposed by Büchter et al. [3]. It has been chosen for two reasons; on one hand, the geometrical nonlinearity can be written in a quadratic form, which allows us to apply easily the perturbation techniques and to obtain the fastest algorithm. On the other hand, this formulation uses a 3D constitutive law without condensation, which allows us to implement nonlinear constitutive laws in an easy way.

2.1. Equilibrium

The shell formulation adopted in this study allows us, thanks to the enhanced assumed strain (EAS) concept [21], to use a complete 3D constitutive law without condensation. The principle of this concept is to introduce an additional part of the strain $\tilde{\gamma}$ which is independent on the displacement and orthogonal to the stress field:

$$\gamma - \mathbf{B}\mathbf{u} = \tilde{\gamma}, \qquad \int_v {}^t\mathbf{S} : \tilde{\gamma}\,\mathrm{d}v = 0, \tag{1}$$

where γ is the Green Lagrange strain field, $\mathbf{B}\mathbf{u}$ the compatible part of the strain and $\mathbf{S}$ is the second Piola Kirchhoff stress tensor. The equilibrium condition is expressed by the following relation:

$$\int_v {}^t\mathbf{S} : \delta\gamma\,\mathrm{d}v - P_\mathrm{c}(\delta\mathbf{u}) = 0, \tag{2}$$

where $P_\mathrm{c}(\delta u)$ denotes the virtual work generated by the contact forces and expressed as following:

$$P_\mathrm{c}(\delta u) = \int_{S_\mathrm{c}} \mathbf{R}\cdot\delta\mathbf{u}\,\mathrm{d}s, \tag{3}$$

where S_c and $\mathbf{R}$ denote respectively the contact surface and the contact forces. In the present study, the contact forces are the only external loads.

2.2. Constitutive law

In this study, we do not take into account the elastic unloading, so we adopt the deformation theory of plasticity which is convenient for the application where the physical nonlinearity is more important than the effect of the irreversible process and of the history of the loading. In this work, we choose an elastoplastic constitutive law based on the Ramberg–Osgood relation which is written in the 3D case in the following form [10]:

$$E\gamma = (1+v)\mathbf{S}^\mathrm{d} - (1-2v)P\mathbf{I} + \frac{3}{2}\alpha\left[\frac{S_\mathrm{eq}}{\sigma_y}\right]^{n-1}\mathbf{S}^\mathrm{d}, \tag{4}$$

where E, v, α, n, $\mathbf{S}^\mathrm{d}$, P, $\mathbf{I}$ and σ_y respectively relate the Young's modulus, the Poisson's ratio, the yield offset, the hardening exponent, the stress deviator, the equivalent hydrostatic pressure ($P = -(1/3)\mathbf{S}:\mathbf{I}$), the unit matrix and the yield stress. As the hardening exponent is not an integer, this relation is not analytic for a null stress, a regularization procedure is introduced by slightly modifying the equivalent Mises stress S_eq. In order to make easier the power series application, a differential relation is introduced:

$$\begin{aligned}
&\bullet\ E(1+\alpha(\eta_\mathrm{m})^n)\gamma = (1+v)\mathbf{S}^\mathrm{d} - (1-2v)P\mathbf{I} + \kappa\mathbf{S}^\mathrm{d},\\
&\bullet\ \zeta^2 = \frac{3}{2\sigma_y^2}\mathbf{S}^\mathrm{d}:\mathbf{S}^\mathrm{d} + (\eta_\mathrm{m})^2,\\
&\bullet\ \zeta\,\mathrm{d}\kappa = (n-1)\kappa\,\mathrm{d}\zeta,
\end{aligned} \tag{5}$$

where η_m denotes the regularization parameter of the constitutive law, κ and ζ are two intermediate variables defined as follows:

$$\kappa = \frac{3}{2}\alpha\left[\frac{S_{eq}}{\sigma_y}\right]^{n-1} = \frac{3}{2}\alpha\zeta^{n-1}. \tag{6}$$

For more details concerning this subsection, readers are referred to [1] and [28].

2.3. Contact problem

The contact sheet-tool is assumed to be an interaction between a deformable body and a rigid one that can move during the process. This interaction adds new sources of difficulties in the numerical simulation due to the nonlinear aspect of the boundary conditions [19]. In the literature, different formulations for the treatment of the contact problem have been proposed. The well known formulations are the penalty method and the Lagrange multipliers one. In the penalty method, a penalized functional is introduced, hence the initial constrained problem is transformed into an unconstrained one. In this method, the penalty parameter must be large to satisfy approximately the nonpenetration condition. Furthermore, this leads to an ill-conditioning of the stiffness matrix. The main advantage of this method is the simplicity of the implementation. The Lagrange multipliers technique consists in introducing a new field to the functional of the problem, which increases the number of the unknowns and then the number of equations to be solved. The appearance of a block of zeros in the diagonal of the tangent operator can lead to a numerical instability during the computation process. The main advantage of this method is that the boundary conditions are exactly satisfied [29]. The other methods are generally based on these two latter: we can quote the perturbed Lagrange multipliers and the augmented Lagrange multipliers, barrier method [22].

In the literature, the contact problem remains the most sensitive problem by means of the several conditions to be satisfied and the care that must be taken to ensure the convergence of the solution with a reasonable computing time, especially in 3D models, where the increase in the number of contact points causes a considerable reduction in time increment size [16].

The application of the ANM to the frictionless contact problem has shown its efficiency in Elhage-Hussein et al. [11] work. To develop a modelling using shell elements, we have extended this work to a three dimensional case and taken into account the displacements of the rigid bodies (denoting tools) during the process.

The classical unilateral contact conditions are expressed by

$$(\mathbf{R}\cdot\mathbf{n})h = 0, \qquad \mathbf{R}\cdot\mathbf{n} \geqslant 0,\ h \geqslant 0, \tag{7}$$

where $\mathbf{R}$, h and $\mathbf{n}$ respectively denote the contact force, the current clearance and the normal in the current point. These conditions are not analytic, so to apply a perturbation technique, they are replaced by the following hyperbolic relationship:

$$\mathbf{R}h = \eta_c(\delta - h)\mathbf{n}, \tag{8}$$

where δ and η_c respectively denote the initial clearance and the contact regularization parameter. The regularized relation between the contact force $\mathbf{R}$ and the clearance h is depicted in Fig. 1. One notices that for η_c sufficiently small, this law sticks with the perfect one. Likely the hyperbolic relation (8), proposed in [11], is the simplest analytic law, that can be brought arbitrarily near the perfect unilateral contact condition (7). In the contact literature, there are many ways to regularize the unilateral law (7). A quite similar regularization has been applied recently by Kloostersman et al. [22], but in a quite different context. Indeed in [22], the hyperbolic distance-multiplier relation is replaced by a linear function in the case of a strong penetration: this results in a C^1 relation, i.e. a C^2 Lagrangian functional, and not an analytical relation as required here. But the computational algorithm is the main difference between the two approaches: in the

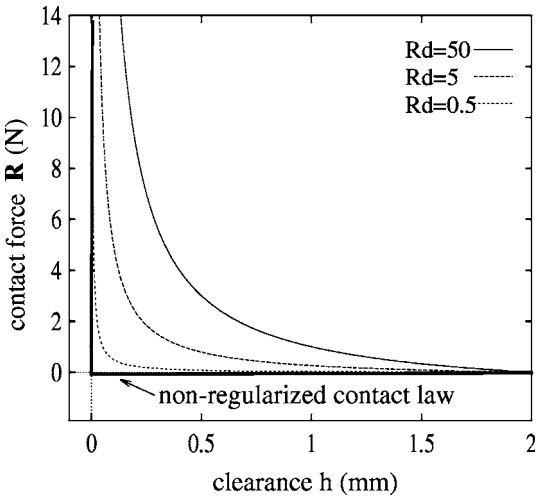

Fig. 1. Contact law regularization with different values of contact parameters R_d ($h_d = 0.05$).

present paper, the regularization (8) defines a new contact law and the global problem is solved by ANM continuation, while, in [22], the regularization appears only in the internal loop of an iterative algorithm to solve the exact unilateral contact problem. The regularized law (8) has been chosen to avoid any penetration. To allow for such a penetration, the following modified law could be used, as presented and discussed in [23], where the number K is a sort of tool stiffness:

$$(R + Kh)R = \eta_c(\delta - h). \tag{9}$$

As the contact conditions introduce h and $\mathbf{n}$ as supplementary unknowns, complementary equations are needed to solve the contact problem. These equations are given by taking into account the geometry of the rigid bodies. In this study, we limit ourselves to a simple rigid body shape. To represent the punch, considered as the principal tool in the 3D hemispherical stretching model, we choose a spherical rigid body (Fig. 2). This model, considered as a standard manufacturing process, was used experimentally by Ghosh

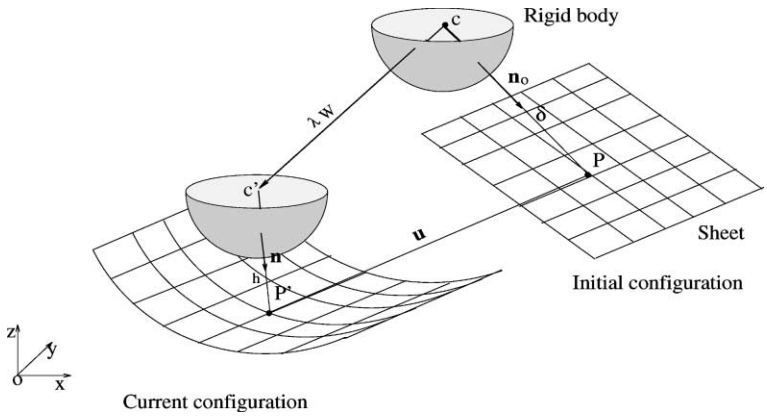

Fig. 2. 3D modelling of the contact problem: case of a spherical rigid body submitted to an arbitrary displacement.

and Hecker [7] and has been numerically treated, for the first time, by Wang and Budiansky [26] in a model based on an axisymmetric membrane shell finite element formulation [9].

In the considered hemispherical stretching problem, the deformation is only due to the displacement of the rigid body, that will be chosen here in the form $\lambda\mathbf{w}$, where the direction $\mathbf{w}$ is prescribed and the real parameter λ is the control parameter of the problem. A point P of the structure defined by the position vector $\mathbf{X}$ and the initial contact parameters $(\delta, \mathbf{n}_0)$ in the initial configuration occupies the position P' in the current configuration after a displacement $\mathbf{u}$ (Fig. 2). So, we can express the clearance and the normal by these two quadratic equations:

$$(h+\rho)^2 = \langle \mathbf{X}+\mathbf{u}-\mathbf{C}-\lambda\mathbf{w}, \mathbf{X}+\mathbf{u}-\mathbf{C}-\lambda\mathbf{w}\rangle, \tag{10}$$

$$(h+\rho)\mathbf{n} = (\mathbf{X}+\mathbf{u}-\mathbf{C}-\lambda\mathbf{w}). \tag{11}$$

We denote by ρ, $\mathbf{X}$ and $\mathbf{C}$ respectively the punch radius, a vector defining the initial position of the current point and a vector defining the initial position of the rigid body. These two Eqs. (10) and (11) could be substituted into Eq. (8) to obtain an expression of the contact force $\mathbf{R}$ as a function of the displacement and of the control parameter λ only. In this study, the contact problem is assumed to be frictionless.

3. Perturbation technique

3.1. Computing a step of the solution path

In this section, we apply the asymptotic method to solve the global problem corresponding to the equilibrium Eq. (2), the compatibility condition (1), the constitutive law (5) and the contact relations (8, 10 and 11). So, we apply a perturbation technique which consists in expanding all the variables of the problem into power series. We denote by $\mathbf{U} = (\mathbf{u}, \gamma, \tilde{\gamma}, \mathbf{S}, h, \mathbf{n}, \mathbf{R})$ the global unknown vector. This vector as well as the control parameter λ are expanded into power series with respect to a path parameter "a":

$$\begin{cases} \mathbf{U}(a) = \mathbf{U}_0 + a\mathbf{U}_1 + a^2\mathbf{U}_2 + \cdots, \\ \lambda(a) = \lambda_0 + a\lambda_1 + a^2\lambda_2 + \cdots. \end{cases} \tag{12}$$

The introduced parameter "a", which represents an additional unknown, is similar to the control parameter of the classical iterative algorithms. We choose to define it by the following classical expression [5]:

$$a = \langle \mathbf{u}-\mathbf{u}_0, \mathbf{u}_1\rangle + (\lambda-\lambda_0)\lambda_1. \tag{13}$$

Substituting this set of Eqs. (12) and (13) into those governing the problem (equilibrium, constitutive relation and compatibility) and by identifying like powers of "a", we obtain a recurrent sequence of well posed linear problems, which will be solved by a finite element method until a series truncation order p. These linear problems will have the same tangent stiffness matrix. We then obtain an analytical representation of a part of the solution branch with only one stiffness MD, which is very significant for strongly nonlinear problems and problems with large sizes.

The development of the equilibrium and the compatibility equations until a series truncation order p gives:

$$\int_v \left\{ {}^t\mathbf{S}_0 : 2\gamma_{nl}(\mathbf{u}_p, \delta u) + {}^t\mathbf{S}_p : (\gamma_l(\delta u) + \gamma_{nl}(\mathbf{u}_0, \delta u)) \right\} \mathrm{d}v + \int_v \sum_{r=1}^{p-1} {}^t\mathbf{S}_r : 2\gamma_{nl}(\mathbf{u}_{p-r}, \delta u)\,\mathrm{d}v - \int_{S_c} \mathbf{R}_p^c\,\delta u\,\mathrm{d}s = 0, \tag{14}$$

$$\int_v {}^t\mathbf{S}_p : \delta\tilde{\gamma}\,\mathrm{d}v = 0. \tag{15}$$

Then the expansions of the constitutive law lead to these two equations:

$$\begin{cases} \text{order } 1 : \mathbf{S}_1 = \mathbf{D}_t : \gamma_1, \\ \text{order } p : \mathbf{S}_p = \mathbf{D}_t : \gamma_p + \mathbf{S}_p^{\text{res}}, \end{cases} \tag{16}$$

where $\mathbf{D}_t$ is the tangent stiffness tensor and $\mathbf{S}_p^{\text{res}}$ is a sort of residual stress (for more details see [28]). The stress expressions are substituted into the equilibrium equations to obtain problems with the displacement field as the main unknown.

After expansion into power series and identification of like powers of the parameter "a", the contact conditions (8, 10 and 11) give the following expressions:

At order 1:

$$\begin{cases} h_1 = \dfrac{\langle \mathbf{X} + \mathbf{u}_0 - \mathbf{c} - \lambda_0 \mathbf{w}, \mathbf{u}_1 - \lambda_1 \mathbf{w} \rangle}{h_0 + \rho}, \\ \mathbf{n}_1 = \dfrac{(\mathbf{u}_1 - \lambda_1 \mathbf{w})}{h_0 + \rho} - \dfrac{h_1 \mathbf{n}_0}{h_0 + \rho}, \\ \mathbf{R}_1 = \dfrac{\eta(\delta - h_0)}{h_0} \mathbf{n}_1 - \dfrac{h_1}{h_0} (\eta \mathbf{n}_0 + \mathbf{R}_0). \end{cases} \tag{17}$$

At order p:

$$\begin{cases} h_p = \dfrac{\langle \mathbf{X} + \mathbf{u}_0 - \mathbf{c} - \lambda_0 \mathbf{w},\ \mathbf{u}_p - \lambda_p \mathbf{w} \rangle}{h_0 + \rho} + \dfrac{1}{2} \displaystyle\sum_{r=1}^{p-1} \dfrac{\langle \mathbf{u}_{p-r} - \lambda_{p-r} \mathbf{w}, \mathbf{u}_r - \lambda_r \mathbf{w} \rangle - h_r h_{p-r}}{h_0 + \rho}, \\ \mathbf{n}_p = \dfrac{\mathbf{u}_p - \lambda_p \mathbf{w} - h_p \mathbf{n}_0}{h_0 + \rho} - \displaystyle\sum_{r=1}^{p-1} \dfrac{h_r \mathbf{n}_{p-r}}{h_0 + \rho}, \\ \mathbf{R}_p = \dfrac{\eta(\delta - h_0)}{h_0} \mathbf{n}_p - \dfrac{h_p}{h_0} (\eta \mathbf{n}_0 + \mathbf{R}_0) - \displaystyle\sum_{r=1}^{p-1} \dfrac{h_r}{h_0} (\eta \mathbf{n}_{p-r} + \mathbf{R}_{p-r}). \end{cases} \tag{18}$$

One notes that after substituting the clearance h_p and the normal $\mathbf{n}_p$ into the contact force, this latter will depend only on the displacement field and on the load parameter λ, which will make easy the finite element discretization.

3.2. Padé approximants

In the ANM literature, the series representation has been improved by replacing the polynomial approximations by rational ones named Padé approximants [11,17]:

$$\begin{cases} \mathbf{U}(a) = \mathbf{U}_0 + a \dfrac{D_{n-2}}{D_{n-1}} \mathbf{U}_1 + a^2 \dfrac{D_{n-3}}{D_{n-1}} \mathbf{U}_2 + \cdots + a^{n-1} \dfrac{1}{D_{n-1}} \mathbf{U}_{n-1}, \\ \lambda(a) = \lambda_0 + a \dfrac{D_{n-2}}{D_{n-1}} \lambda_1 + a^2 \dfrac{D_{n-3}}{D_{n-1}} \lambda_2 + \cdots + a^{n-1} \dfrac{1}{D_{n-1}} \lambda_{n-1}, \end{cases} \tag{19}$$

where $D_i(a)$ are polynomials of degree (i) with real coefficients $(d_i)_{[i=1,n-1]}$:

$$D_i(a) = 1 + a d_1 + a^2 d_2 + \cdots + a^i d_i. \tag{20}$$

It has been proved in [12] and [2] that these rational representations increase significantly the range of validity of the polynomial series which permits a considerable reduction of the computing time.

Hereafter, in the numerical applications, the presented results correspond to an ANM algorithm based upon the Padé approximants. Indeed, in this work, this technique has been implemented and has improved significantly the validity range as compared to the ANM algorithm based upon polynomial series. In most cases the rational representations allow one a reduction of about 50% of the number of steps needed to achieve the computation.

3.3. Finite element discretization

After perturbation technique and discretization by finite element method, the problem at order p is written as follows:

$$[\mathbf{Kt}]\{\mathbf{u}_p\} = \{\mathbf{F}_p^{\mathrm{nl}}\} + \{\mathbf{R}_p^r\}, \tag{21}$$

where $[\mathbf{Kt}]$ denotes the contactless tangent stiffness matrix computed at the initial solution $(\mathbf{U}_0, \lambda_0)$, $\{\mathbf{u}_p\}$ is the discretized displacement vector at order p, $\{\mathbf{F}_p^{\mathrm{nl}}\}$ is the classical right-hand side within the ANM. In this study, this vector and the matrix $\mathbf{Kt}$ have the same expression as the one used in [28]. As it has been done in [11], the vector $\{\mathbf{u}_p\}$ is decomposed into two components $\{\mathbf{u}_p\} = \{\mathbf{u}_p^{\mathrm{c}}, \mathbf{u}_p^{\mathrm{nc}}\}$, where $\{\mathbf{u}^{\mathrm{c}}\}$ is the displacement of the contact nodes and $\{\mathbf{u}^{\mathrm{nc}}\}$ is the displacement of the other ones. The vector $\{\mathbf{R}_p^r\} = \{\mathbf{R}_p^{\mathrm{c}}, 0\}$ representing the contact force can be expressed in the following form:

$$\{\mathbf{R}_p^{\mathrm{c}}\} = [\mathbf{Ktc}]\{\mathbf{u}_p^{\mathrm{c}}\} + \lambda_p\{\mathbf{F}^{\mathrm{c}}\} + \{\mathbf{F}_p^{\mathrm{nlc}}\}, \tag{22}$$

where $[\mathbf{Ktc}]$ is a symmetric contact stiffness matrix, $\{\mathbf{F}^{\mathrm{c}}\}$ is a force vector that depends on the prescribed displacement vector $\mathbf{w}$ and $\mathbf{F}_p^{\mathrm{nlc}}$ a vector which depends nonlinearly on contact terms computed at previous orders.

The problem is discretized using a shell element. It is a quadrilateral eighth nodes element and, to ensure the development of the yielding and of the elastoplastic bending response, five Gauss integration points through the thickness direction are used. For more details about the shell finite element adopted in the present study and the strategy of the contact algorithm, readers can refer to [11,27].

3.4. Continuation procedure

As the validity range of series is limited, a continuation procedure had been proposed by Cochelin [5] to describe the whole solution path in a step by step manner. At each step, the maximal value of the path parameter 'a' is defined automatically. A simple criterion is to require that the difference between the solutions at two consecutive orders remains below a given value $\epsilon 1$:

$$\text{range of validity } a_{\mathrm{m}} = \left(\epsilon_1 \frac{\|\mathbf{u}_1\|}{\|\mathbf{u}_p\|}\right)^{1/(p-1)}. \tag{23}$$

Here, we apply a continuation technique based on the Padé approximants, that has been recently proposed by Elhage-Hussein et al. [12]. In this case, the range of validity ($a_{\mathrm{m}p}$) of the solution is defined by the following expression:

$$\epsilon_2 \simeq \frac{\|\mathbf{P}_n(a_{\mathrm{m}p}) - \mathbf{P}_{n-1}(a_{\mathrm{m}p})\|}{\|\mathbf{P}_n(a_{\mathrm{m}p}) - \mathbf{u}_0\|}, \tag{24}$$

where the maximal value $a_{\mathrm{m}p}$ of the path parameter "a" is sought in the interval $[a_{\mathrm{m}},$ first pole] and determined by some bisection iterations. The first pole is the smallest real root of the denominator D_{n-1} of Eq. (19).

4. Numerical results

The proposed algorithm has been applied to simulate the 3D hemispherical stretching. In this study, we compare the results with those obtained with the help of the industrial code Abaqus which uses an updated Lagrangian formulation and the Newton method coupled with the Lagrange multipliers when the contact conditions are involved.

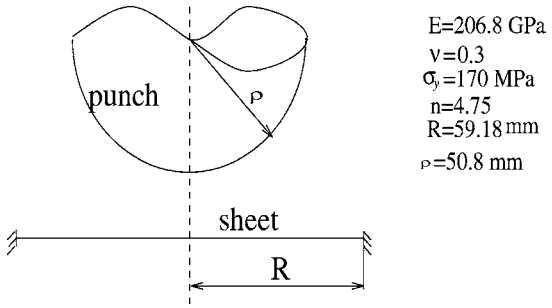

Fig. 3. Hemispherical deep-drawing process: geometry and mechanical properties.

In Fig. 3, we show the geometry and the mechanical properties used in this study. The sheet is 1 mm thick, has a circular shape and supposed to be clamped at its edges. Given the symmetry of the structure, it is sufficient to model only a quarter for the computation. The considered blank is made of aluminium-killed steel, which is assumed to satisfy the Ramberg–Osgood stress–strain relation (4).

The structure is discretized into the shell (8 nodes) element mentioned previously. In Fig. 4 the deformed mesh is displayed, it corresponds to a vertical punch displacement of 27.8 mm.

In Fig. 5, we report the equivalent Mises stress versus the loading parameter λ which allows the control of the punch displacement. Curves correspond to the integration point located near the sheet center. Fig. 6 shows the punch force-travel evolution. This force corresponds to the total contact force. We can notice that we are able to obtain a very good estimation of the drawing force and of the stress.

4.1. Optimal truncation order of series

To look for the optimal order, we have studied for different orders the CPU time needed to reach the solution path. For three sizes of the problem (600, 1537 and 5766 dof) corresponding respectively to the tables of Figs. 7–9, we present for each considered order, the number of steps required to achieve the computation, the ratio between the time necessary to evaluate the right-hand sides **Fnl** and the time $t1$ needed for the evaluation and the decomposition of the tangent stiffness matrix **Kt** and finally the total relative time corresponding to the ratio between the total CPU time and the time $t1$. We notice that the

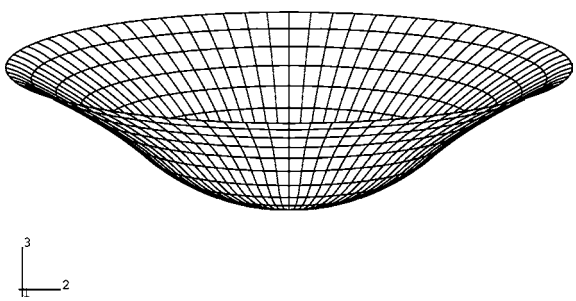

Fig. 4. Deformed configuration of the sheet after a punch travel of 27.8 mm. In the computation, symmetry conditions are taken into account and only a quarter of the sheet is considered.

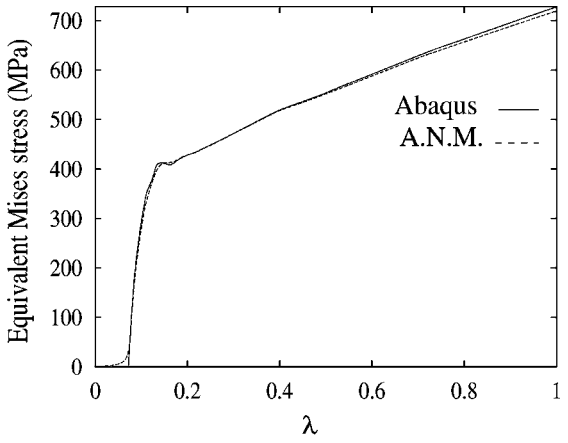

Fig. 5. Evolution of the equivalent Mises stress versus the load parameter (λ): comparison with the industrial code Abaqus.

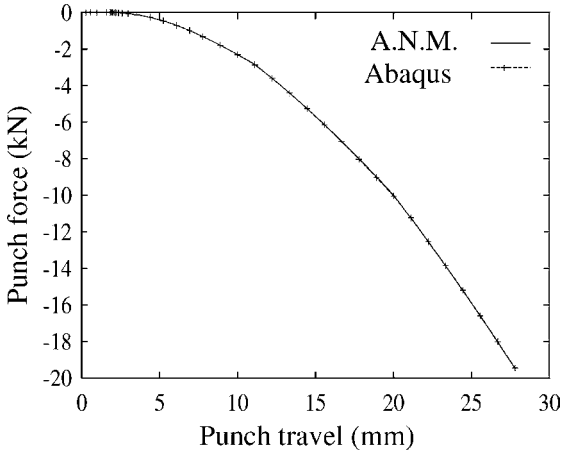

Fig. 6. Evolution of the punch force versus the travel (it corresponds to the total equivalent contact force): comparison with Abaqus.

Order	Nb step	$\frac{t(Fnl)}{t(Kt)}$	Total relative time
8	110	0.49	163.90
12	73	0.85	135.05
13	**68**	**0.95**	**132.60**
14	64	1.08	133.12
15	61	1.19	133.59
20	50	1.85	142.50

Fig. 7. Study of the CPU time: determination of the optimal order in a problem of 600 dof. Computer used HP 9000/712.

Order	Nb step	$\frac{t(Fnl)}{t(Kt)}$	Total relative time
8	94	0.52	142.88
12	63	0.84	115.92
13	**59**	**0.94**	**114.46**
14	57	1.04	116.28
15	54	1.26	122.04
20	44	1.88	126.72

Fig. 8. Study of the CPU time: determination of the optimal order in a problem of 1537 dof. Computer used HP 9000/712.

Order	Nb steps	$\frac{t(Fnl)}{t(Kt)}$	Total relative time
8	86	0.54	132.85
12	60	0.93	115.57
13	**55**	**1.01**	**110.56**
14	53	1.14	113.31
15	51	1.23	113.89
20	43	1.83	121.69

Fig. 9. Study of the CPU time: determination of the optimal order for a problem with 5766 dof. Computer used HP 9000/712.

obtained optimal order is 13. This result is in good agreement with some results in the ANM literature where the optimal order varies between 10 and 15 and the corresponding ratio t**Fnl**/t**Kt** is often close to 1.

As we have introduced two regularization parameters in the present algorithm, a contact regularization parameter (here noted η_c) and a material one (noted η_m), we propose to study the effect of these parameters on the quality of the solution as well as on the computing time.

4.2. Influence of the material regularization

We have undertaken four computations with different values of the material regularization parameter ($\eta_m = 1, 0.1, 0.01$ and 0.001) introduced in formula (5). We have observed that for the three values (0.1, 0.01 and 0.001) the algorithm gives about the same quality of the solution and with the same number of MDs (39 MDs). A value $\eta_m = 1$ of the regularization parameter induces an unacceptable modification of the global response curve (Fig. 10). This is not surprising because this leads also to a strong modification of the constitutive law. In what follows, we keep the value $\eta_m = 0.1$.

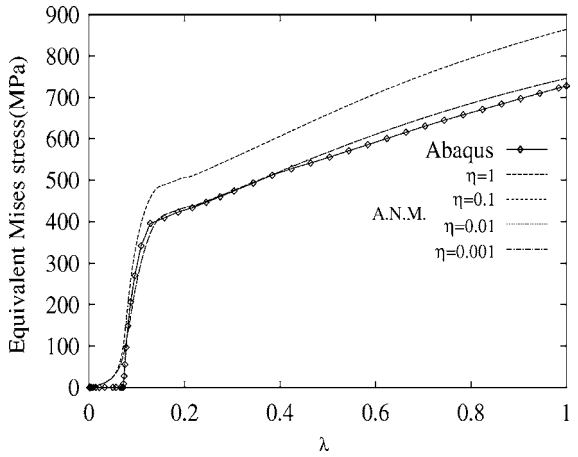

Fig. 10. The equivalent Mises stress for different values of the material regularization parameter.

4.3. Influence of the contact regularization

If the material regularization parameter η_m can be chosen more or less arbitrarily in a wide range, it is known that the contact regularization has to be defined carefully [2,11]. The regularized contact law involves the initial clearance δ that is function of the material point $\mathbf{X}$, so that the regularization can be not uniform along the contact surface. To homogenize the contact regularization, we define a parameter η_c depending on the contact point as in [11]

$$\eta_c(\mathbf{X}) = \frac{R_d h_d}{\delta(\mathbf{X}) - h_d}, \tag{25}$$

where h_d is a typical and given distance ($h_d = 0.05$ in our calculation) and R_d is a typical and given contact force. We shall make vary this force R_d to define a strong or a weak regularization. For the same problem studied above, and the same mesh density (600 dof), we compare the results for $R_d = 5$ and $R_d = 0.5$ with the one obtained by the help of Abaqus.

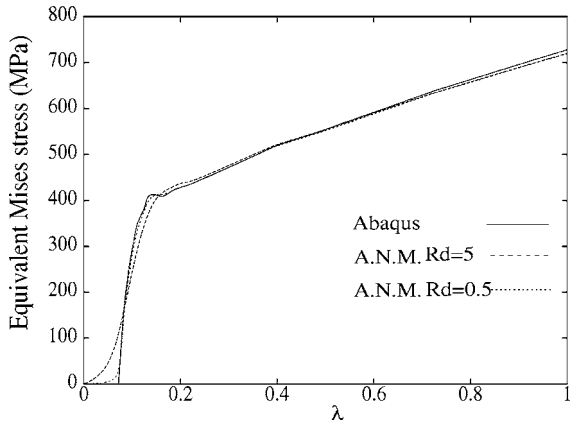

Fig. 11. Comparison of the equivalent Mises stress: influence of the contact regularization parameter on the solution quality ($h_d = 0.05$).

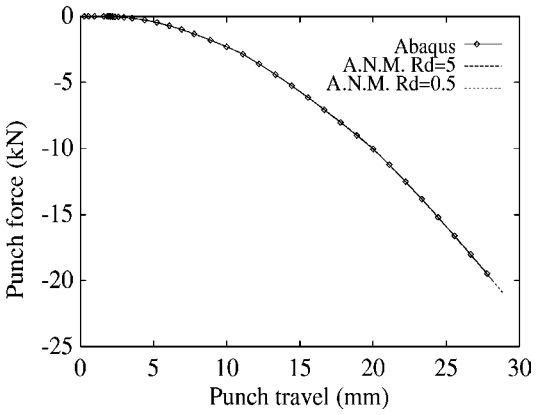

Fig. 12. Comparison of the punch force: influence of the contact regularization parameter on the solution quality ($h_d = 0.05$).

Rd=5	Rd=0.5
39	68

Fig. 13. Influence of the contact regularization parameter R_d ($h_d = 0.05$), number of MDs needed to reach a punch depth of 27.8 mm for a problem of 600 dof.

One notices that the contact regularization parameter (R_d) has a significant influence on the accuracy of the solution. As it is shown in Fig. 11, smaller the parameter R_d is, better is the quality of the solution. This is not the case when we deal with the punch force corresponding to the global contact force as it is shown in Fig. 12. Indeed, on the contrary to the local variable (for example stress), the total contact one (global variable) is directly related to the total equilibrium which is satisfied even with large values of the contact regularization parameter.

Now what is the effect of these regularization parameter values on the computing time, i.e., the fastness of the algorithm?

In Fig. 13, we show the effect of the contact regularization on the fastness of the algorithm. We notice that the number of steps, corresponding to the number of MDs, increases for small values of the contact regularization parameter. Indeed, when the regularization parameter (R_d) is small the nonlinearity becomes very strong, so more steps are needed to obtain the solution path. In what follows, we retain the value $R_d = 0.5$ to get a sufficient accuracy in the calculation of the local variable.

4.4. Efficiency of the present algorithm

The problem has been treated for three meshes involving respectively 600, 1536 and 5766 degrees of freedom and using the shell element presented previously. In the table of Fig. 14, we compare the number of MDs needed to reach a punch displacement of 27.8 mm.

We notice that the mesh refinement makes more difficult the convergence of the iterative methods (Abaqus) contrary to the ANM algorithm which preserves its efficiency. Note that for a large size problem, the number of points in contact with the tool is great. This induces an ill-conditioning of the tangent matrix for iterative algorithms which leads to a slower convergence and induces a great number of **Kt** decompositions as it is shown in the table of Fig. 14. Contrary to the iterative algorithms, the ANM remains

d.o.f.	A.N.M.	Abaqus
600	68	185
1536	59	197
5766	55	326

Fig. 14. Number of the MDs: ANM, compared to Abaqus, truncation order of series 13, $R_d = 0.5$, $\epsilon 1 = \epsilon 2 = 10^{-7}$.

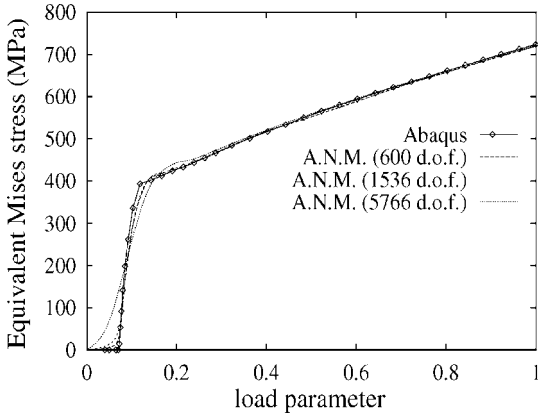

Fig. 15. Equivalent Mises stress: influence of the mesh refinement on the solution quality, comparison with Abaqus.

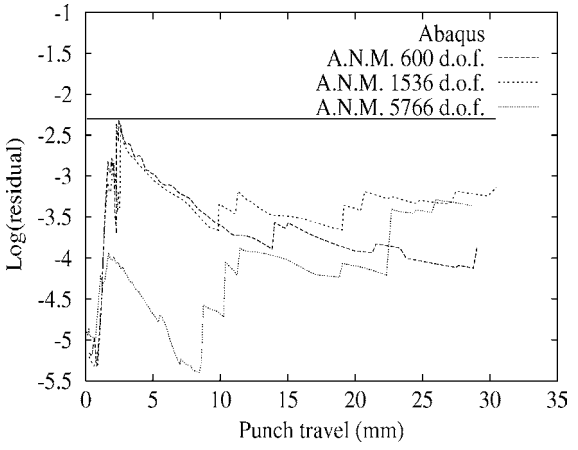

Fig. 16. The residual versus the punch travel evolution along the process: comparison with Abaqus.

efficient for a large problem size, which is due to the special treatment of the contact conditions. This result is very important in problems dealing with the numerical simulation of material forming processes where several nonlinearities are combined. Furthermore, the problems treated have generally large sizes and a very fine mesh is often required to reach satisfactory solutions.

We note that these results are obtained by using the same contact regularization (R_d, h_d). One remarks a slight reduction of the ANM number of steps when the size of the problem, i.e. the number of the contact points, increases. This is due to the following fact. After discretization, each node of the slave surface is submitted to a contact force **Rc**. When the mesh is made finer, the global contact force remains about constant and therefore the nodal contact forces are reduced. Thus an increase of the mesh density is more or less equivalent to a softening of the regularization,so the nonlinearity becomes smooth (Fig. 15). In this figure, we notice that in spite of this phenomenon, accuracy of the solution remains very good for the three considered meshes.

A common strategy within ANM is to choose sufficiently small accuracy parameters to limit the increase of the residual along the solution path. The obtained residual has been plotted in Fig. 16, with the choices $\epsilon 1 = \epsilon 2 = 10^{-7}$. One can observe that we have got a much better accuracy than the industrial code, that requires a maximum residual of about 5×10^{-3} after iterations. Thus the studied problem can be solved without correction phases and with a very good accuracy.

5. Concluding remarks

In this paper, we have presented an ANM to solve problems coupling several nonlinearities. As an example, we have chosen a 3D simulation of the hemispherical stretching which involves nonlinearities due to geometry, plasticity and contact conditions. We have limited ourselves to a material model based on the deformation theory of plasticity as well as simple tool shapes and frictionless contact model. The 3D hemispherical stretching is a well known benchmark for the numerical simulation of sheet metal forming. In view of this type of application, it should be interesting to account for many material and technical data, for instance anisotropy and friction. Unfortunately, this is not necessary so long as an efficient and reliable ANM algorithm has not been established for more consistent models of plasticity.

In this work, we have emphasized the efficiency of the ANM to deal with contact conditions. The classical iterative algorithms present generally some numerical problems (instability, penetration, large computing time...). The algorithm presented in this work does not increase the size of the stiffness matrix and does not allow the penetration phenomenon. It is very convenient for problems with a great number of contact points, which is always the case in the simulation of sheet forming processes.

The obtained results show the accuracy of the present method and especially its efficiency when the size of the problem becomes very large and the number of contact points increases. Compared to the industrial code Abaqus used as a reference, the ANM needs less MDs and then less computing time. The reason of this performance is the ability of the method to decompose only one stiffness matrix by step and to adjust automatically the step size according to the local nonlinearity encountered.

References

[1] B. Braikat, N. Damil, M. Potier-Ferry, Méthodes asymptotiques numériques pour la plasticité, Rev. Europ. Eléments Finis 6 (1997) 337–357.

[2] J. Brunelot. Simulation de la mise en forme à chaud par une méthode asymptotique numérique. Thesis, Université de Metz, France, 1999.

[3] N. Büchter, E. Ramm, D. Roehl, Three dimensional extension of non-linear shell formulation based on the Enhanced Assumed Strain Concept, Int. J. Numer. Meth. Engrg. 37 (1994) 2551–2568.

[4] J.M. Cadou, B. Cochelin, N. Damil, M. Potier-Ferry, ANM for stationary Navier–Stokes equations and with Petrov–Galerkin formulation, Int. J. Numer. Meth. Engrg. 50 (2001) 825–845.

[5] B. Cochelin, A path-following technique via an asymptotic-numerical method, Comput. Struct. 53 (1994) 1181–1192.

[6] B. Cochelin, N. Damil, M. Potier-Ferry, The asymptotic-numerical method: an efficient perturbation technique for non-linear structural mechanics, Rev. Europ. Eléments Finis 3 (1994) 281–297.

[7] A. Ghosh, S.S. Hecker, Failure in thin sheets stretched over rigid punches, Metall. Trans. 6A (1975) 1065–1074.
[8] F.M. Guerra, R.V. Browing, Comparison of two slideline methods using adina, Comput. Struct. 17 (1983) 819–834.
[9] ABAQUS, Examples problems manual, version 5.8, 1998, Hibbitt, Karlsson, and Sorenson, 1080 Main St., Pawtucket, RI 02860–4847, USA.
[10] ABAQUS, Theory and users' manuals, version 5.8, 1998, Hibbitt, Karlsson, and Sorenson, 1080 Main St., Pawtucket, RI 02860–4847, USA.
[11] A. Elhage Hussein, N. Damil, M. Potier-Ferry, An asymptotic numerical algorithm for frictionless contact problems, Rev. Europ. Eléments Finis 7 (1998) 119–130.
[12] A. Elhage Hussein, M. Potier-Ferry, N. Damil, A numerical continuation method based on Padé approximants, Int. J. Solids Struct. 37 (2000) 6981–7001.
[13] M. Jean, G. Touzot, Implementation of unilateral contact and dry friction in computer codes with large deformations problems, J. Méc. Théor. Appl. special issue 7 (1988) 145–160.
[14] C. Kallala. Approche géométrique du contact entre solides par la méthode des éléments finis. Thesis, ENSAM (Paris), France, 1993.
[15] N. Kikuchi, J.T. Oden, Contact problems in elastostatics, in: J.T. Oden, G.F. Carey (Eds.), Finit Elements, vol. 5, 1984.
[16] J.C. Nagtaal, L.M. Taylor, Comparison of Implicit and Explicit Finite Element Methods for Analysis of Sheet Forming Problems, VDI BERICHTE, 1991, pp. 705–725, no. 894.
[17] A. Najah, B. Cochelin, N. Damil, M. Potier-Ferry, A critical review of asymptotic numerical methods, Arch. Comput. Meth. Engrg. 5 (1998) 31–50.
[18] B. Nour-omid, P. Wriggers, A two-level iteration method for solution of contact problems, Comput. Methods Appl. Meth. Engrg. 54 (1986) 131–144.
[19] E. Oñate, C. Agelet de Saracibar, Alternatives for finite element analysis of sheet metal forming problems, in: Chenot, Wood, Zienkiewicz (Eds.), Proceedings of Numerical Methods in Industrial Forming Processes, 1992, pp. 79–88.
[20] M. Potier-Ferry, N. Damil, B. Braikat, J. Descamps, J.M. Cadou, H.L. Cao, A. Elhage Hussein, Traitement des fortes non-linéarités par la méthode asymptotique numérique, CR Acad. Sci. Paris t.324 (Série II b) (1997) 171–177.
[21] J.C. Simo, M.S. Rifai, A class of mixed assumed strain methods and method of incompatible modes, Int. J. Numer. Meth. Engrg. 37 (1990) 1595–1636.
[22] G. Kloosterman, R.M.J. van Damme, A.H. van den Boogaard, J. Huétink, A geometrical-based contact algorithm using a barrier method, Int. J. Numer. Meth. Engrg. 51 (2001) 865–882.
[23] H. Abichou, Simulation de l'emboutissage à froid par une méthode asymptotique numérique. Thesis, Université de Metz, France, 2001.
[24] J. Descamps, H.L. Cao, M. Potier-Ferry, An asymptotic numerical method to solve large strain viscoplastic problems, in: Barcelona, D.J.R. Owen, E. Hinton, E. Oñat (Eds.), Proceedings of the 5th Conference on 'Computational Plasticity, Fundamentals and Applications', 1997, pp. 393–400.
[25] A. Tri, B. Cochelin, M. Potier-Ferry, Résolution des équations de Navier-Stokes et détection des bifurcations stationnaires par une méthode asymptotique numérique, Rev. Europ. Eléments Finis 5 (4) (1996) 415–442.
[26] N.M. Wang, B. Budiansky, Analysis of sheet metal stamping by a finite element method, J. Appl. Mech. 45 (1978) 73–82.
[27] H. Zahrouni, B. Cochelin, M. Potier-Ferry, Computing finite rotations of shells by an asymptotic-numerical method, Comput. Methods Appl. Mech. Engrg. 175 (1999) 71–85.
[28] H. Zahrouni, M. Potier-Ferry, H. Elasmar, N. Damil, Asymptotic numerical method for nonlinear constitutive laws, Rev. Europ. Eléments Finis 7 (1998) 841–869.
[29] Z.H. Zhong, Finite Element Procedure for Contact-Impact Problems, Oxford University, Oxford, 1993.